International Journal of Pressure Vessels and Piping 206 (2023) 105047

Contents lists available at ScienceDirect

International Journal of Pressure Vessels and Piping

journal homepage: www.elsevier.com/locate/ijpvp

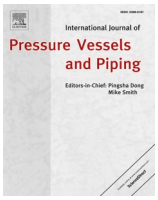

An estimation method (LOESS) for dealing with the imperfections of existing parametric creep models for time to failure: Illustrated using 2.25Cr–1Mo steel

Mark Evans

Institute of Structural Materials, Swansea University Bay Campus, SA1 8EN, Swansea, Wales, UK

ARTICLE INFO

Keywords:
LOESS estimation
Creep
Parametric models
Cross validation

ABSTRACT

It is important to be able to predict the creep life of materials used in power plants. This paper illustrates the inadequacies of existing parametric creep models in achieving this aim for 2.25Cr–1Mo steel. This breakdown occurs due to different creep mechanisms being present at different test conditions. This paper puts forward a locally weighted estimation technique (LOESS) to tackle this problem that importantly maintains the parametric model's structure by using local (to the test condition) weighted regression procedures. It was observed that this technique not only produces more sensible values for key parameters such as the activation energy, but it also produces much more accurate predictions of lifetimes close to operating conditions when using only short-term data (less than 10,000 h) to quantify the creep model's unknown parameters. The variation in the model's creep parameters with stress were also consistent with previous studies on the changing creep mechanisms for this material.

1. Introduction

It is important to be able to predict the creep life of materials used in power plants and aeroengines. When this can be done with a high degree of confidence, the results can potentially be used to justify the continued use of aging power plants beyond their original design lives as a short-term solution to potential energy gaps. 2.25Cr–1Mo is a main stay steel used for structural components operating at high temperature within such aging power plants - where the usual service conditions for heater tubes is around 823 K and 35 MPa. Yet, it has proved very challenging to predict the service life of this material at such conditions using just the results from accelerated tests (tests done at higher stresses and temperatures). This is because the dominant creep mechanism for this material appears to change with stress. An early study on this material by Maruyama et al. [1] identified three separate stress regimes for the MAF batch of 2.25Cr–1Mo steel in Creep Data Sheet 3B &50 [2,3], published by the Japanese National Institute for Materials Science. (These data sheets have numerous batches of this steel each of which were subjected to a different heat treatment and had a different chemical composition. The composition of the MAF batch was in wt.%: Fe – 2.46 Cr – 0.94Mo – 0.1C–0.23Si – 0.43Mn – 0.011P – 0.009S–0.008Ni – 0.07Cu – 0.005Al). A more recent study by Wilshire and Whittaker [4] also identified three different stress regimes. Indeed, changing creep mechanisms are a major cause of creep models failing to accurately predict creep life at operating conditions based on accelerated test data.

Both above-mentioned studies normalised the stress. The study by Maruyama et al. [1] normalised the stress by dividing it through by the Young's modulus values quoted in their paper and then the minimum creep rate was made a power law function of this normalised stress. In contrast, Wilshire and Whittaker [4] normalised by dividing the stress through by the tensile strength for the material and the minimum creep rate was then made a power law function of the reciprocal of this log normalised stress. In both models' failure time was temperature compensated using an Arrhenius relation. In each model there was no evidence found for an activation energy that varied with stress and temperature (but different activation energies were identified by these authors that is likely the result of the different normalisation of stress that was used in each case - with $Q_c = 421$ kJmol^{-1} in the Maruyama et al [1]. and $Q_c = 230$ kJmol^{-1} in the Wilshire and Whittaker [4] study).

Despite this difference, the creep mechanism identified in each stress regime was very similar in each paper. The high stress regime corresponded to stresses above the materials yield stress where new dislocations multiply rapidly during the initial strain on loading, i.e. plastic deformation takes place by a dislocation glide mechanism. Thereafter,

E-mail address: m.evans@swansea.ac.uk.

https://doi.org/10.1016/j.ijpvp.2023.105047
Received 5 June 2023; Received in revised form 7 August 2023; Accepted 8 August 2023
Available online 10 August 2023

dislocation creep begins where the main obstacle to their movement is the changed dislocation substructure upon high stress loading. In the medium stress regime, where the stress is below the yield stress, specimens deform elastically upon loading and the dislocation substructure remains almost as it was before testing begins. Dislocation creep must occur not so much by the generation of new dislocations but more by the movement of the dislocations pre-existing in the as received bainitic microstructure. Dislocation creep is therefore present from the start with the main obstacles to their movement being precipitates such as M_2C-type carbides. The initial plastic deformation present in the high stress regime gives rise to bigger creep rates relative to the medium stress regime, so that any reduction in stress will then results in smaller increases in life relative to the medium stress regime. The lowest stress regime is characterised by very long test durations that degrades the initial bainitic microstructure - the original lath-like structure entirely disappears. This causes the creep rate to increase sharply, compared to that in the intermediate stress regime, so that any reduction in stress will then results in smaller increases in life relative to the medium stress regime. Fig. 1 shows the three stress regimes identified by Maruyama et al.'s [1].

Some solutions to this problem of changing creep mechanisms are present in the literature. A recent approach taken by Ding et al. [5], is to specify a separate equation to explain creep rates due to grain boundary sliding, dislocation creep and dislocation glide. The overall creep rate is then simply the sum of the creep rates predicted by these mechanisms. Integration using true stress and true strain then yields an expression for predicting the observed creep curve at any point in time based on these evolving creep mechanisms. The approach is readily extended to encompass other mechanisms - for example including a role for high temperature oxidation. By modelling the whole creep curve, this approach can predict the role of both primary creep and microstructure evolution on time to failure. As an alternative to the specification of different equations for different creep mechanisms is to use the same creep model but apply it over a limited range of test conditions where the mechanism is constant, and then allow the parameters of this single model to change at more divergent test conditions. Changing parameter values within a single creep equation then account for changing creep mechanisms. Whilst this more empirical approach has the advantage of simplicity, it is not able to model the role of primary creep on time to failure - although the role of microstructure evolution is revealed by the changing patterns of the model's parameters.

The alternative approach taken by Bolton [6] is to accepted that many parametric creep models are correctly specified with respect to temperature but are incorrectly specified with respect to stress. Consequently, the stress – failure time relationship given by a particular model is replaced with cubic piece-wise splines. However, the use of such splines place limits on the extent to which extrapolations can be made with respect to stress and so a life prediction at the service stress may not always be possible. The alternative is to adopt the approach typically used when working with the Wilshire model [4]. Here the relationship between stress and failure time implied by the model is maintained, so enabling unlimited extrapolative ability. But it is accepted that this relationship holds over a more limited range of test conditions and will change as the creep mechanism changes with stress. Use of the Wilshire model has therefore involved fitting two or more linear lines (each line corresponding to a different creep mechanism) to the data, with the model parameters changing abruptly at specific stress values. This approach was only ever meant to be an approximation, as it implies an instantaneous change in creep mechanism at these specific stress values. However, the dominance of the creep mechanisms identified above change gradually with test conditions.

The locally weighted regression and smoothing scatterplots procedure (LOESS) developed by Cleveland [7] can be seen as fitting within the Wilshire approach, but overcomes the issue of abrupt changes in creep mechanism. The idea behind this semi parametric procedure is that the relationship between failure time and stress suggested by a model is valid, but only over a narrow range of test conditions where the creep mechanism is constant. The result is a smooth curve to represent the

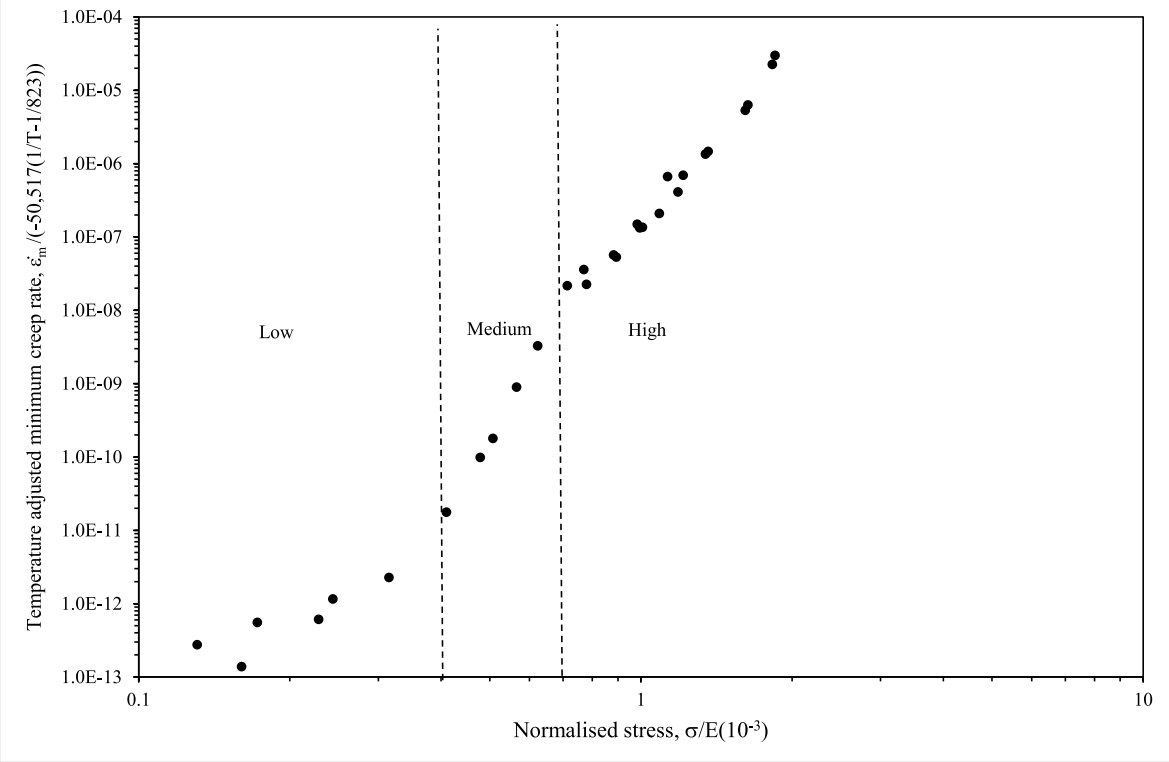

Fig. 1. Relationship between stress (σ), Young's modulus (E) and $\dot{\varepsilon_m}/\left[50,517\left(\frac{1}{T}-\frac{1}{823}\right)\right]$ for the MAF batch of 2.25Cr–1Mo steel contained in NIMS creep data sheets 3B & 50 [2,3].

relationship between these variables - which is more consistent with the fact that the dominance of the above identified creep mechanisms change slowly, and not abruptly, with respect to test conditions. By still using the model equations relating stress to failure time, this approach also places no limits to the degree of extrapolation.

This paper therefore has two main aims. The first is to demonstrate the inadequacy of some well-known parametric creep models in predicting long term data from short term data. Given this finding, the paper then demonstrates the improved predictive capability that comes with the use of LOESS. To this end the paper is structured as follows. The next section summarises the data set on 2.25Cr–1Mo that is used in this paper The following section summarises the main parametric creep models to be found in the literature, discusses how the unknown parameters are estimated and evaluates their predictive capabilities. The penultimate section then applies LOESS to the data to demonstrate its improved predictive capabilities. The paper finishes with a conclusion section suggesting some areas for future research.

2. The data

This paper makes use of information in Creep Data Sheet 3B & 50, published by the Japanese National Institute for Materials Science (NIMS) [2,3]. This has extensive data on twelve batches of 2.25Cr–1Mo (according to JIS STBA 23, Grade 22) steel where each batch has a different chemical composition that underwent one of four different heat treatments - details of which are given in Ref. [2]. This paper makes use of just one of these batches, the MAF batch, which was in tube form and had an outside diameter of 50.8 mm, a wall thickness of 8 mm and a length of 5000 mm with a chemical composition of (in wt.%): Fe – 2.46 Cr – 0.94Mo – 0.1C–0.23Si – 0.43Mn – 0.011P – 0.009S–0.008Ni – 0.07Cu – 0.005Al. Specimens for creep testing were taken longitudinally from this material. Each test specimen had a diameter of 6 mm with a gauge length of 30 mm.

The creep tests were obtained over a wide range of conditions: 400 MPa - 22 MPa and 723 K–923 K. For the MAF batch (and only this batch) both minimum creep rates and time to failure measurements were recorded, together with the times to attain various strains - 0.005, 0.01, 0.02 and 0.05. Fig. 2 plots the creep failure times obtained for this MAF batch at the different stresses and temperatures used. The relationship between time to failure and test conditions is quite complicated for this batch - which has made it very difficult to model and predict such failure times using well known parametric creep models.

3. Parametric creep models

3.1. Structure and characteristics

Table 1 summarises several well-known parametric models for predicting creep life. All the models predict a particular characteristic of the creep curve such as its end point or the minimum slope along the creep curve. The Orr-Sherby-Dorn (OSD) [8] and Larson-Miller (LM) [9] models have as their basis the Arrhenius relation

$$\dot{\varepsilon}_m = A\exp\left(-\frac{Q_c}{RT}\right) \tag{1a}$$

where $\dot{\varepsilon}_m$ is the minimum creep rate measured from several creep curves obtained from tests carried out at different absolute temperatures T, but at the same constant stress (σ) or load. Q_c is the activation energy for creep, R is the universal gas constant and A is an unknown constant. The end point of a creep curve is then predicted by combining this with the Monkman-Grant [10] relation (assuming the power exponent on the minimum creep rate equals unity)

$$t_F = \frac{M}{\dot{\varepsilon}_m} = A^* \exp\left(\frac{Q_c}{RT}\right) \tag{1b}$$

where M is a further model parameter that is material dependent, $A^* = M/A$ and t_F is the time to failure. In the OSD model the parameter A^* is made a function of stress, $A^* = f_{OSD}(\sigma)$

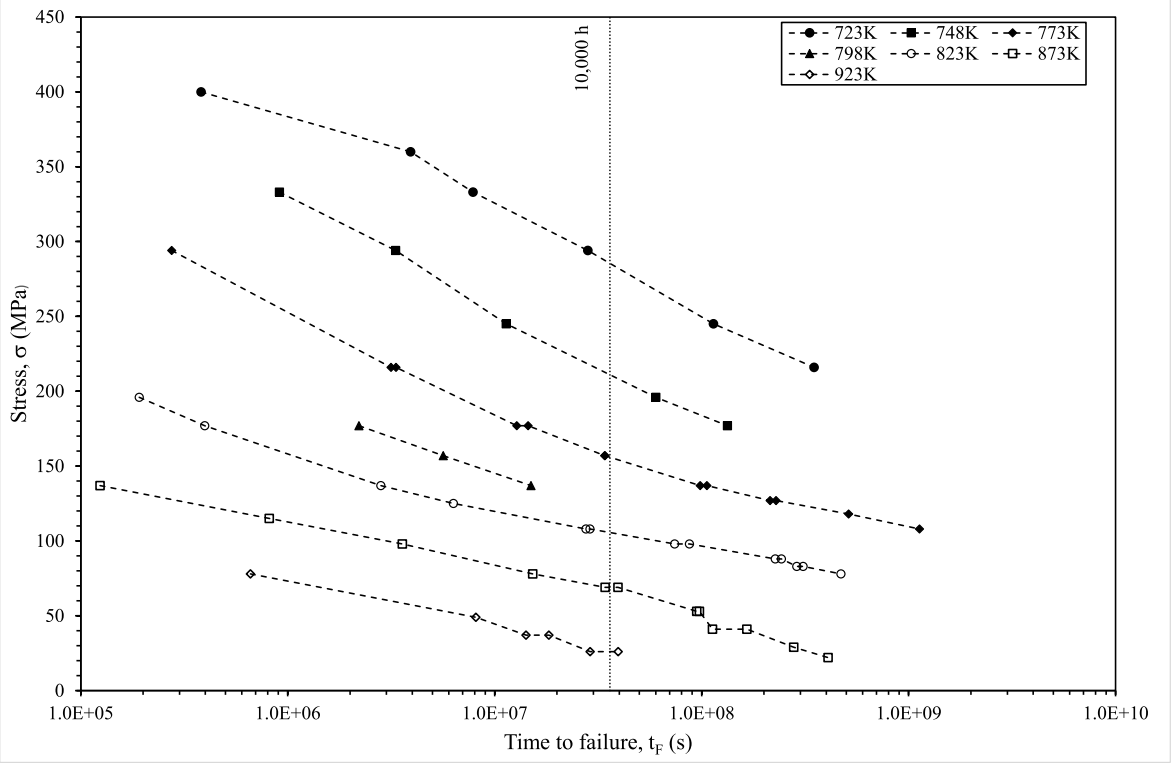

Fig. 2. Relationship between stress, temperature, and time to failure for the MAF batch of 2.25Cr–1Mo steel contained in NIMS creep data sheet 3B &50 [2,3].

Table 1
Parametric creep models.

Model name (Authors)	Model specification	Equation No.
Orr-Sherby-Dorn [8] (OSD)	$\ln(t_F) = \ln(B) + n\ln(\sigma) + \frac{Q_c}{R}\left(\frac{1}{T}\right)$	(2a)
	$\ln\left(t_{F,o}\right) = \ln\left(t_F\right) + \frac{Q_c}{R}\left(\frac{1}{T_0} - \frac{1}{T}\right)$	(2b)
	$\ln(\sigma_o) = \ln(\sigma)$	(2c)
Larson-Miller [9] (LM)	$\ln\left(t_F\right) = \ln(A^*) + \frac{a_0}{R}\frac{1}{T} + \frac{a_1}{R}\frac{\ln(\sigma)}{T}$	(3a)
	$\ln\left(t_{F,o}\right) = \frac{T}{T_o}\ln\left(t_F\right) - \ln(A^*)\left[\frac{T}{T_o} - 1\right]$	(3b)
	$\ln(\sigma_o) = \ln(\sigma)$	(3c)
Manson-Haferd [11] (MH)	$\ln(t_F) = [\ln(A^*) - a_2T_a] + a_2T + a_3T\ln(\sigma) - a_3T_a\ln(\sigma)$	(4a)
	$\ln\left(t_{F,o}\right) = \left\{\frac{[T_o - T_a]}{[T - T_a]}\right\}\ln(t_F) + \ln(A^*)\left[1 - \left\{\frac{[T_o - T_a]}{[T - T_a]}\right\}\right]$	(4b)
	$\ln(\sigma_o) = \ln(\sigma)$	(4c)
Wilshire [4] (W)	$\ln\left(t_F\right) = \ln(B^*) + n^*\ln\left[\ln\left(\frac{\sigma_{TS}}{\sigma}\right)\right] + \frac{Q_c}{R}\frac{1}{T}$	(5a)
	$\ln\left(t_{F,o}\right) = \ln\left(t_F\right) + \frac{Q_c}{R}\left[\frac{1}{T_o} - \frac{1}{T}\right]$	(5b)
	$\ln(\sigma_o) = \ln(\sigma) + \ln(\sigma_{TS,o}/\sigma_{TS})$	(5c)
Evans [12] (E)	$\ln(t_F) = \ln(B^*) - n^*\ln\left(\frac{\sigma_{max}}{\sigma} - 1\right) + \frac{Q_c}{R}\frac{1}{T}$	(6a)
	$\ln(t_{F,o}) = \ln\left(t_F\right) + \frac{Q_c}{R}\left[\frac{1}{T_o} - \frac{1}{T}\right]$	(6b)
	$\ln(\sigma_o) = \ln(\sigma) + \ln(\sigma_{max,o}/\sigma_{max})$	(6c)
Soviet model [16] (SM)	$\ln\left(t_F\right) = \ln(D) + a_4\ln(T) + a_5\ln(\sigma) + Q_c\frac{1}{RT} + a_6\frac{\ln(\sigma)}{T}$	(7a)
	$\ln\left(t_{F,o}\right) = \ln\left(t_F\right) - (a_4 + a_5)\ln\left(\frac{T}{T_o}\right) + Q_c\left(\frac{1}{RT_o} - \frac{1}{RT}\right)$	(7b)
	$\ln(\sigma_o) = \ln(\sigma) - \ln(T/T_o)$	(7c)
Minimum Commitment Method [14] (MCM)	$\ln(t_F) = b_0 + b_1T + db_2\frac{1}{T} + b_3\sigma + b_4\ln(\sigma)$	(8a)
	$\ln\left(t_{F,o}\right) = \ln\left(t_F\right) + b_1(T_o - T) + b_2\left(\frac{1}{T_o} - \frac{1}{T}\right)$	(8b)
	$\ln(\sigma_o) = \ln(\sigma)$	(8c)

$$t_F = f_{OSD}(\sigma)\exp\left(\frac{Q_c}{RT}\right) \tag{1c}$$

In the LM model, it is Q_c that is made a function of stress $Q_c = f_{LM}(\sigma)$

$$t_F = A^*\exp\left(\frac{f_{LM}(\sigma)}{RT}\right) \tag{1d}$$

The Manson-Haferd (MH) [11] model is like the LM [9] model except that it replaces 1/T with T – T_a, where T_a is a particular value for T

$$t_F = A^*\exp\left(\frac{T - T_a}{f_{MH}(\sigma)}\right) \tag{1e}$$

In all these models, the functional stress relationship is left unspecified so that the literature is full of different variations of these models, i.e., differing in the specification of the stress functions. Table 1 shows some specific variants of these three models. Eq. (2a) of Table 1 assumes $f_{OSD}(\sigma) = B\sigma^n$ where B and n are further model constants. Eq. (3a) of Table 1 assumes $f_{LM}(\sigma) = a_0 + a_1\ln(\sigma)$ where a_0 and a_1 are further model constants. Eq. (4a) of Table 1 assumes $1/f_{MH}(\sigma) = a_2 + a_3\ln(\sigma)$ where a_2 and a_3 are further model constants. But other variants of these models assume linear or polynomial functions in stress or log stress.

The foundations of the Evans model [12] is to be found in Eq. (1c) with $f_{OSD}(\sigma) = B^*\left(\left[\frac{\sigma_o}{\sigma} - 1\right]\right)^{-n*}$, where σ_o is a reference stress. In the Evans model, the reference stress is σ_{max} - the maximum strength a material can withstand whilst stretching before breaking. If a tensile test is conducted at a high enough strain rate so that the resulting measured tensile strength (σ_{TS}) is invariant to the strain rate, then σ_{max} can be replaced by σ_{TS}. This is the assumption made in the Wilshire model - Eq. (5a) in Table 1 (where a different stress transformation is also used). Otherwise σ_{max} is another model parameter leading to the Evans model and Eq. 6(a) in Table 1.

Some of the differences between Eqs. (2a-5a) are illustrated in Fig. 3. Fig. 3a is a schematic iso-stress representation of the OSD model. The log of t_F varies in a linear fashion with 1/T at a particular value for stress, and changing stress leads to a parallel shift in the iso-stress lines. Fig. 3b is a schematic iso-stress representation of the LM model. Log t_F again varies in a linear fashion with 1/T at a particular value for stress, and changing stress leads to a change in the slope of the iso-stress lines. Irrespective of the stress, the log failure time is predicted to equal ln(A*) when 1/T = 0. Fig. 3c is a schematic iso-stress representation of the MH model. Ln t_F now varies in a linear fashion with T at a particular value for stress, and changing stress leads to a change in the slope of the iso-stress lines. Irrespective of the stress, the log failure time is predicted to equal ln(A*) when T = T_a. Fig. 3d is a schematic iso-stress representation of the Evans model. Ln(t_F) now varies in a linear fashion with 1/T at a particular value for the normalised stress σ/σ_{max} and changing this normalised stress leads to a parallel shift in the iso -stress lines.

The Soviet model is more closely related to Eyring's [13] rate theory

$$t_F = DT^{a_4}\exp\left(\frac{Q_c}{RT} + f(T,\sigma)\right) \tag{1f}$$

Eq. (7a) of Table 1 is obtained by letting $f(T,\sigma) = \left(a_5 + a_6\frac{1}{T}\right)\ln(\sigma)$

The Minimum Commitment method (MCM) [14] model shown as Eq. (8a) in Table 1 is perhaps the simplest variant that has been applied in the literature with other versions including, for example, the square of stress. It cannot be directly related to the Arrhenius or Eyring equations.

The parametric models can either be expressed using a single equation (equation numbers ending in "a" in Table 1) or equivalently as two separate equations (equation numbers ending in "b" and ""c in Table 1). These dual equations simply convert a specimens failure time obtained at any stress σ and at temperatures different To, into when the specimen would have failed if tested at the same stress but at temperature T_o (where T_0 is an arbitrarily chosen base line temperature). Bolton [6], and latter Cano et al. [15], have termed T_o the datum temperature. All but two of the models are converted to a baseline temperature by just temperature compensating the time to failure. But the Evans [12] and Soviet [16] models also require the stress to be temperature compensated. For these models, there therefore exists an effective stress, σ_0. For example, in the Evans model the effect of stress on failure time is dependent on how close that stress is to the maximum strength. Due to the strain rate dependency of tensile or maximum strength at high temperatures, instantaneous failure may not always occur at the σ_{TS} values quoted in various data bases (and used frequently in the Wilshire model). Instead, instantaneous failure will occur at σ_{max} which needs to be estimated from the failure time data. But because these strengths (σ_{TS}, σ_{max}) are in turn dependent on temperature, this effective stress varies with temperature. Thus, the application of a stress equal to 300 MPa at 823 K, is not equivalent to the application of 300 MPa at 923 K. It is the normalised stresses σ/σ_{max} that are equivalent over different temperatures. That is, $\sigma/\sigma_{max} = \sigma_o/\sigma_{max,o}$ where $\sigma_{max,o}$ is the maximum strength of a specimen experiencing a temperature equal to the baseline temperature.

3.2. Parameter estimation

Before any predictions can be made, the unknown parameters of any parametric creep model must be estimated. Two approaches can be taken. Notice that the single equation representations of the creep

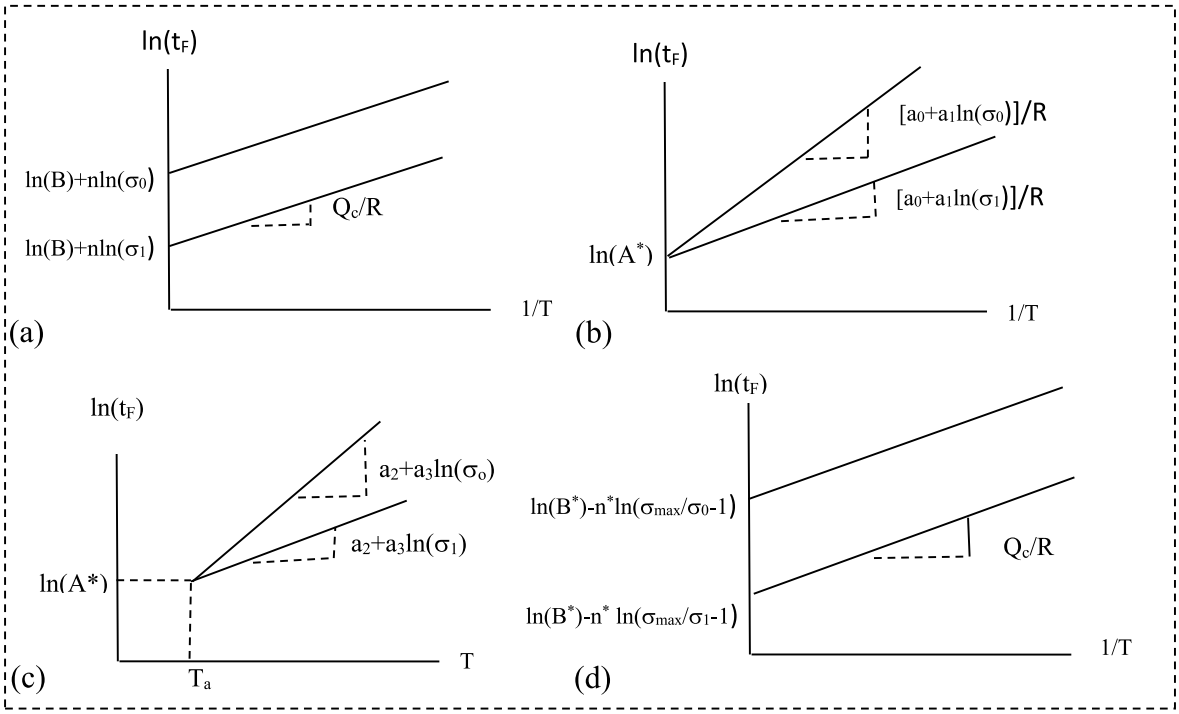

Fig. 3. Schematic representation of iso-stress lines for (a) the OSD model, (b) the LM model, (c) the MH model and (d) the Evans model. Stress σ_1 > stress σ_0.

models (equation numbers ending in "a" in Table 1) are all linear in the unknown parameters and so these can be estimated using multiple linear least squares. If the dual equation representations are used (equation numbers ending in "b,c" in Table 1) a two-step non-linear least squares procedure must be used. The first step is the same for all models shown in Table 1. It involves a multiple linear regression of the equations ending in "a" in Table 1 to get starting values for some of the unknown model parameters in these equations. The second step refines these starting values using a non-linear search procedure (for this paper this will be done using Excel's Solver [17] subroutine). The specifics of this second step differs from model to model.

For example, in the OSD model, applying multiple least squares to Eq. (2a) will yield an estimate for B, n and Q_c. The latter of these is taken as a starting value for Q_c which is then used in Eq. (2b) to convert all failure times into the baseline failure times $t_{F,o}$ (with $T_o = 823$ K). $\ln(t_{F,o})$ is then regressed on $\ln(\sigma_0)$, (= $\ln(\sigma)$ for this model), to estimate the parameters γ_0 and γ_1 in

$$\ln(t_{F,o}) = \gamma_o + \gamma_1 \ln(\sigma_o) \tag{9a}$$

and from Eq. (2a) the value for γ_o will equal $\left[\ln(B) + \frac{Q_c}{R}\left(\frac{1}{T_0}\right)\right]$ and the value for γ_1 will equal n

$$\ln(t_{F,o}) = \left\{\ln(B) + \frac{Q_c}{R}\left(\frac{1}{T_0}\right)\right\} + n\ln(\sigma_o) \tag{9b}$$

Then in the second step, Solver can be used to find that Q_c value that minimises the residual sum of squares associated with the regression Eq. (9a). The term in squiggly brackets in Eq. (9b) makes it clear what happens in this non-linear search procedure. Namely as Q_c is changed in the search, γ_0 in Eq. (9a) changes to reduce the residual sum of squares. This search continues until Q_c and γ_0 values are found that minimise the residual sum of squares. Once this final Q_c value is identified, the regression Eq. (9b) will yield the optimal values for the other unknown model parameters – n and B (using the optimised value for Q_c and T_o in the identification of the value for B from γ_0).

Table 2 is a summary of how this two-step procedure differs between all the creep models. The second column shows the parameters that require a starting value to find values for $t_{F,o}$ and σ_0. Excel's Solver then changes the values for these parameters to minimise the sum of squared residuals associated with the regression equations shown in column 3 of Table 2. For most models this residual sum of squares is that associated with a linear regression of $\ln(t_{F,o})$ on $\ln(\sigma_0)$, and so will have an intercept and slope term. In the MCM model, $\ln(t_{F,o})$ is regressed on $\ln(\sigma_0)$, σ_0 and σ_0^2. In the W model, $\ln(t_{F,o})$ is regressed on $\ln\left[\ln\left(\frac{\sigma_{TS,o}}{\sigma_o}\right)\right]$. The terms in squiggly bracket in the last column of Table 2, are treated as single

Table 2
Summary of the two-step estimation procedure using the dual equation representation of a parametric creep model.

Model	Starting parameters[a]	Regression equation[b]
OSD	Q_c used in Eq. (2b)	$\ln\left(t_{F,o}\right) = \left\{\ln(B) + \frac{Q_c}{R}\left(\frac{1}{T_0}\right)\right\} + n\ln(\sigma_o)$
LM	A*, T_a used in Eq. (3b)	$\ln(t_{F,o}) = \left\{\ln(A^*) + \frac{a_o}{R}\frac{1}{T_o}\right\} + \left\{\frac{a_1}{RT_o}\right\}\ln(\sigma_o)$
MH	A*, a_2, a_3 used in Eq. (4b)	$\mathrm{Ln}(t_{F,o}) = \{\ln(A^*)+a_2(T - T_a)\} + \{a_3(T - T_a)\}\ln(\sigma_o)$
W	Q_c used in Eqs. (5b,c)	$\ln\left(t_{F,o}\right) = \left\{\ln(B^*) + \frac{Q_c}{R}\frac{1}{T_o}\right\} + n^*\ln\left[\ln\left(\frac{\sigma_{TS,o}}{\sigma_o}\right)\right]$
E	Q_c used in Eqs. (6b,c)	$\ln\left(t_{F,o}\right) = \left\{\ln(B^*) + \frac{Q_c}{R}\frac{1}{T_o}\right\} - n^*\ln\left(\frac{\sigma_{max,o}}{\sigma_o} - 1\right)$
SM	Q_c,a_4,a_5 used in Eqs. (7b,c)	$\ln\left(t_{F,o}\right) = \left\{\ln(D) + a_4\ln(T_o) + Q_c\frac{1}{RT_o}\right\} + \left\{a_5 + \frac{a_6}{T_o}\right\}\ln(\sigma_o)$
MCM	b_1, b_2 used in Eq. (8b)	$\ln\left(t_{F,o}\right) = \left\{b_0 + b_1T_o + b_2\frac{1}{T_o}\right\} + b_3\sigma_o + b_4\ln(\sigma_o)$

[a] In step 1 starting values for the parameters shown in column 2 are used in Table 1 equations ending in b to obtain values for $t_{F,o}$ and σ_o.

[b] In step 2 multiple least squares are used to estimate the parameters of the regression equations shown in column 3. Excel's Solver is then used to find improved values for the starting parameters, i.e., values that minimise the residual sum of squares of the shown regression equations. In minimising this residual sum of squares, the terms in squiggly bracket are treated as a single constant to be estimated using multiple least squares.

constants to be estimated using multiple least squares and simply show how the regression equation changes to minimise the residual sum of squares when Excel's Solver searches for better starting values of the parameters shown in column 2. So, in the SM model, the intercept and slope of the regression line change as Solver searchers for better value for the parameters Q_c and a_4 to a.

3.3. Parametric predictions

Fig. 4 show the results of estimating the baseline temperature representation of a selection of creep models shown in Tables 1 and 2. In all graphs, $t_{F,o}$ is plotted against σ_o, except for the Evans model where $t_{F,o}$ is plotted against $\ln(\sigma_{max,o}/\sigma_o - 1)$. In the estimation process only data points associated with failure times less than 10,000 h are used and these times are shown as solid circles. The open circles are then the longer times to failure. This is done to visualise how well each model does in predicting temperature compensated failure times not "seen" by the parametric models. Fig. 4a shows the OSD model, where the shown prediction line (calculated from only the short-term data) has an R^2 value of 95.83%. The value for Q_c is estimated at around 279 kJmol^{-1}, and the parameter n is estimated at −5.06.

The Z parameter was defined by Holdsworth et al. [18,19] as

$$Z = e^{2.58 s_e} \tag{10a}$$

where s_e is the standard deviation of the difference between the log failure and log predicted temperature compensated times. Ideally, for single-cast assessments these authors suggest Z should be less than or equal to 2, whereas $Z \geq 4$ is unacceptable. The reasoning for this is that if a creep model is assumed to predict the median time to failure at a given test condition, and that failure times at a given test condition follow a normal distribution, and if s_e is also independent of test conditions, then 99% of all failure times will be within the range (where P is the models predicted failure time)

$$\frac{P}{Z} \rightarrow ZP \tag{10b}$$

no matter what the test condition is. Thus, a Z value of 2 means the predictive accuracy of the creep model is such that there is only a 0.5% chance that failure times will be more than 2 times the model's prediction and there is only a 0.5% chance of failure times being lower than half the model's prediction. This is the minimum acceptable level of predictive accuracy according to Holdsworth under these assumptions. A variation of this Z-parameter is given in Fig. 4a

$$Z_{p=0.9} = e^{s_e 1.64} \tag{10c}$$

with the number 1.64 ensuring that $Z_{p\ =\ 0.9}$ defines a set of 90% confidence intervals for the short-term actual failure times. If a well performing model has 99% of actual failure times to within the range given by Eq. (10a,b) with Z at least equal to 2, then this is equivalent to 90% of actual failure times being within the range P/1.55 to1.55$_x$P or smaller (where 1.55 = exp(ln(2)*1.64)/2.58)). Similarly, an unacceptable model has $Z_{p\ =\ 0.9}$ more than 2.4.

For the OSD model in Fig. 4a, $Z_{p\ =\ 0.9}$ equals 3.6 (where s_e is the standard deviation in the difference between the log failure and log predicted temperature compensated times for $t_F \leq 10{,}000$ h). Thus, the track lines show the 5th and 95th percentiles, of a normal distribution (so that under this distributional assumption p = 0.9(100) % of all short term $t_{F,o}$ values should be within the range defined by these lines). So

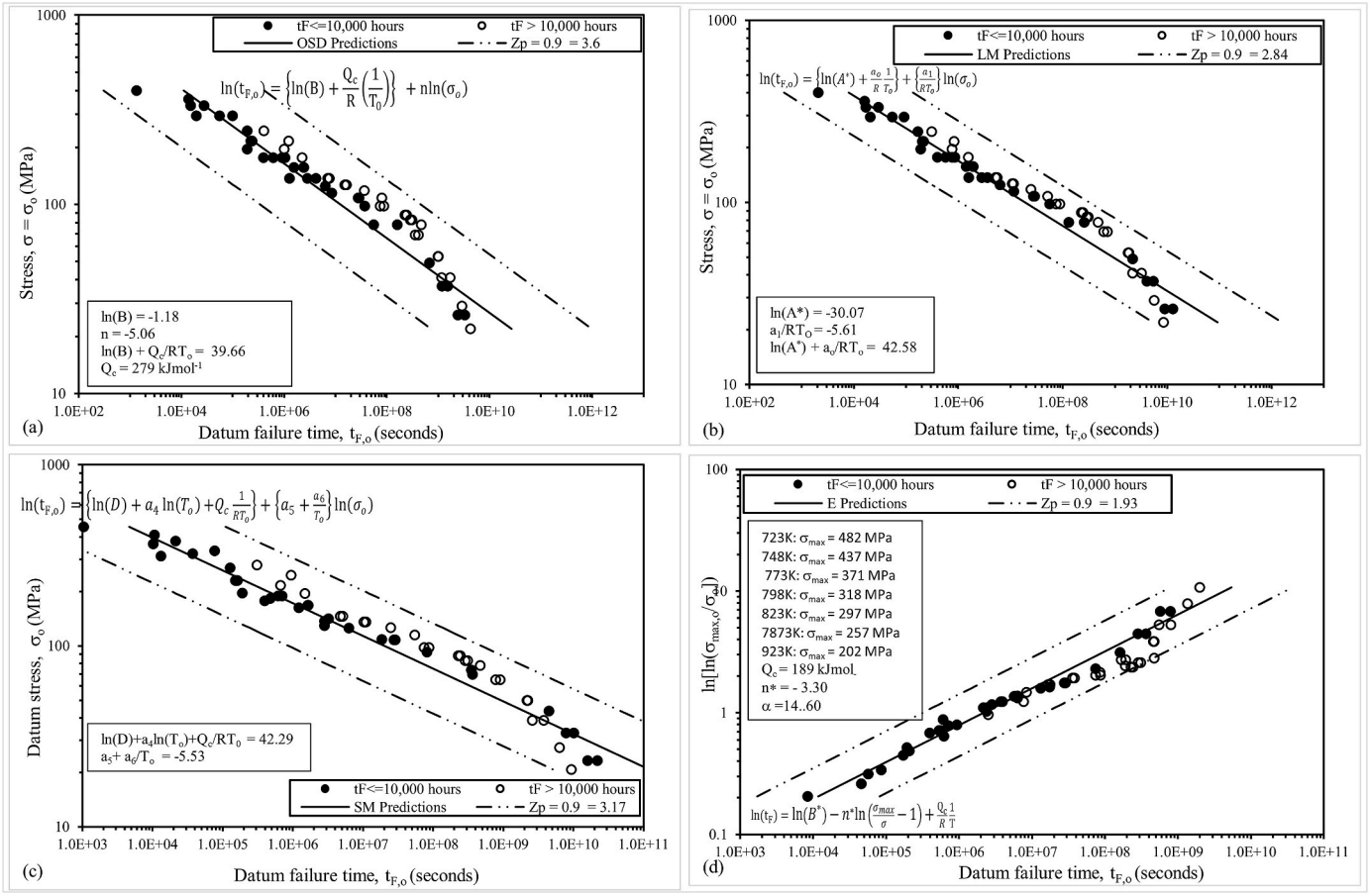

Fig. 4. Relationship between temperature compensated stress and time to failure suggested by (a) the OSD model, (b) the LM model, (c) the Soviet model and (d) the Evans model.

even the fit to the data used in the estimation of the model's parameters are poor as $Z_{p\ =\ 0.9}$ exceeds the maximum acceptable value of 2.4. However, there is also a tendency for the longer-term $t_{F,o}$ values to rise above the short-term values at intermediate stresses, with the opposite occurring at the lowest stresses.

This implies an inability to accurately predict failure times from short-term tests, and this is confirmed in Fig. 5a which plots the predicted failure times against the actual failure times for the longer-term data set only. Ideally, the track lines corresponding to $Z_{p=0.9} = 5.15$ in Fig. 5a should either be on or within the dashed lines corresponding to Z = 1.55. In this extrapolation, the OSD model fails this requirement. The best fit line in Fig. 5a is essentially flattened relative to the 45° line by just those failure times obtained at the lowest two stresses at 873 K (giving an exponent on x(= t_F) of 0.40, which is well below the ideal value of 1. But even if these two points are ignored, the remaining data points are well above the 45° line, giving a constant of 133,694 above the ideal value of 1. Consequently, the OSD model is biased – i.e., consistently under predicts these remaining data points.

Fig. 4b contains the LM model, where the shown prediction line has an R^2 value of 97.70%, and when compared to the OSD model, has a smaller Z_p value of 2.84. The value for ln(A*) is estimated at around −30.07. As is the case with the OSD model, there is a tendency for the long-term data to bulge above the short-term data at intermediate stresses, and bulge below the short-term data at very low stresses. In Fig. 5b, the LM model only performs slightly better than the OSD model with $Z_{p=0.9} = 4.99$ and with the trend line being marginally closer to the 45° line compared to the OSD model. This best fit line is again flattened relative to the 45° line by just two failure times (giving an exponent on x (= t_F) of 0.44, which is well below the ideal value of 1. But even if these two points are ignored, the remaining data points are well above the 45° line, giving a constant of 63,547 above the ideal value of 1.

Fig. 4c contains the SM model, where the shown prediction line has an R^2 value of 97.62%, and Z_p value of 3.17 is in between the values for the previous two models. As is the case with the previous two models, there is a tendency for the long-term data to bulge above the short-term data at intermediate stresses, and bulge below the short-term data at very low stresses. With a $Z_{p=0.9} = 5.63$ in Fig. 5c, the SM model performs worse in extrapolation than either of the previous two models. This best fit line is again flattened relative to the 45° line by just two failure times (giving an exponent on x(= t_F) of 0.39, which is well below the ideal value of 1. But even if these two points are ignored, the remaining data points are well above the 45° line, giving a constant of 155,206 above the ideal value of 1.

Fig. 4d contains the E model, where the shown prediction line has an R^2 value of 98.1%, and Z_p value of 1.93 which is far superior to any of the other three models. As is the case with the previous three models, there is still a tendency for the long-term data to bulge below the short-term data at intermediate stresses. With a $Z_{p=0.9} = 3.56$ in Fig. 5d, the E model performs better in extrapolation than the either of the previous three models. However, the best fit line, has a flatter slope than the 45° line with an exponent on x(= t_F) of 0.55 and a constant of 8060 and is still above the ideal value of 1. There is now a more even spread of data points either side of the 45° line.

The results shown above suggest that, whilst some models performed better in extrapolation than others, none were satisfactory in that the Z_p values for all models exceeded 1.55. All models tended to, on average, underestimate failure times of 10,000 h or more when calibrated using only failure times of less than 10,000 h. In particular, Fig. 4 show that irrespective of the model used to temperature compensate failure times and stresses, the relationship between ln($t_{F,o}$) and ln(σ_o) is not as

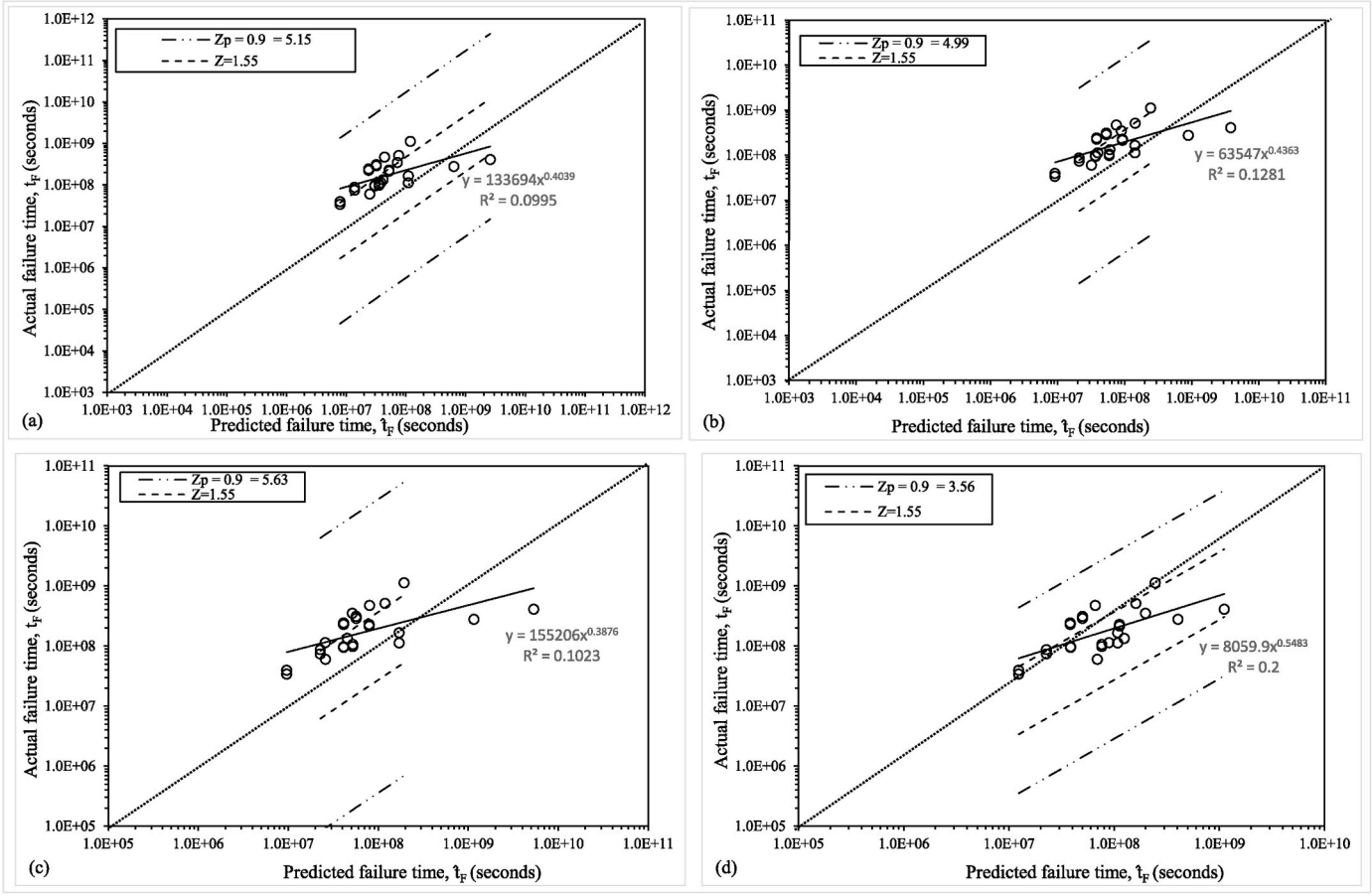

Fig. 5. Actual failure times plotted against the failure times predicted by (a) the OSD model, (b) the LM model, (c) the Soviet model and (d) the Evans model.

described by any model. For example, the OSD, LM and SM models suggest a linear relationship between these two variables, yet the data in Fig. 4 tend to suggest a more complex non-linear relationship. This is also revealed in Fig. 6 that plots the actual failure times against stress, together with the predictions from these four models. As can be seen all models seriously underpredict the actual failure times at all temperatures except at 873 K. Whilst not presented here, the MH, MCM and Wilshire models also suffer from this serious limitation.

4. Semi-parametric (LOESS) models

Lying behind the LOESS semi-parametric technique is the idea that the relationship between $\ln(t_{F,o})$ and $\ln(\sigma_o)$ suggested by a particular parametric creep model is valid, but only over a narrow range of test conditions where the creep mechanism is constant. The result is a smooth curve to represent the relationship between $\ln(t_{F,o})$ and $\ln(\sigma_o)$ which is more consistent with the fact that the dominance of a creep mechanism changes slowly, and not abruptly, with respect to test conditions. By still using the model equations relating stress to temperature, this approach places no limits to the degree of extrapolation.

4.1. Parameter estimation and LOESS predictions of temperature compensated failure times

The technical details behind the LOESS approach are given in the appendix to this paper. But as a summary, the parametric creep model equations are first used to temperature adjust failure times (to create variable y) and stress (to create x) in the same way as that shown in Table 1. As such, the approach used in this paper still accepts that a model describes properly how such adjustments can be made. For one value of x, called the target value for x_o, a weighted regression of ln(y) on ln(x) is then carried out using the qQ nearest data points to x_o (where Q is the number of data points used for estimation (all t_F values below 10,000 h) and q is a fraction of Q). The weights attached to the qQ, y-x pairings, diminish from one (when $x = x_o$) to zero (when x is the furthest from x_0). This is repeated for all values of x in the sample. Thus, LOESS consists of a series of local weighted regressions with each x_o being associated with a unique set of values for the model parameters that are then used to predict the failure time at x_o (and if required for values close to it). The parameters of the model thus change with stress to reflect the changing creep mechanisms. Excel's Solver [17] is used to search for the values of the parameters needed to temperature compensat failure times that minimises the sum sqaured residuals calculated from the Q weighted regressions.

It will always be possible to get better fits to the short-term data by simply reducing q, but such over fitting is likely to result in a loss of generality that will lead to poor extrapolative performance. To prevent such over fitting, the "mis one out cross validation" procedure described in the appendix is used in this paper. In short, the data point associated with each x_0 is omitted from each local regression and the prediction error calculated. These errors are then squared and averaged to give a cross validation (CV) value. The parameter(s) used for temperature compensating stress and time (together with the other model parameters) are then chosen to minimise CV using Excel's Solver. To compare the predictive capability of this LOESS procedure to those obtained in the previous section, this procedure is carried out on failure times up to 10,000 h and the resulting model parameters used to predict these and the longer failure times.

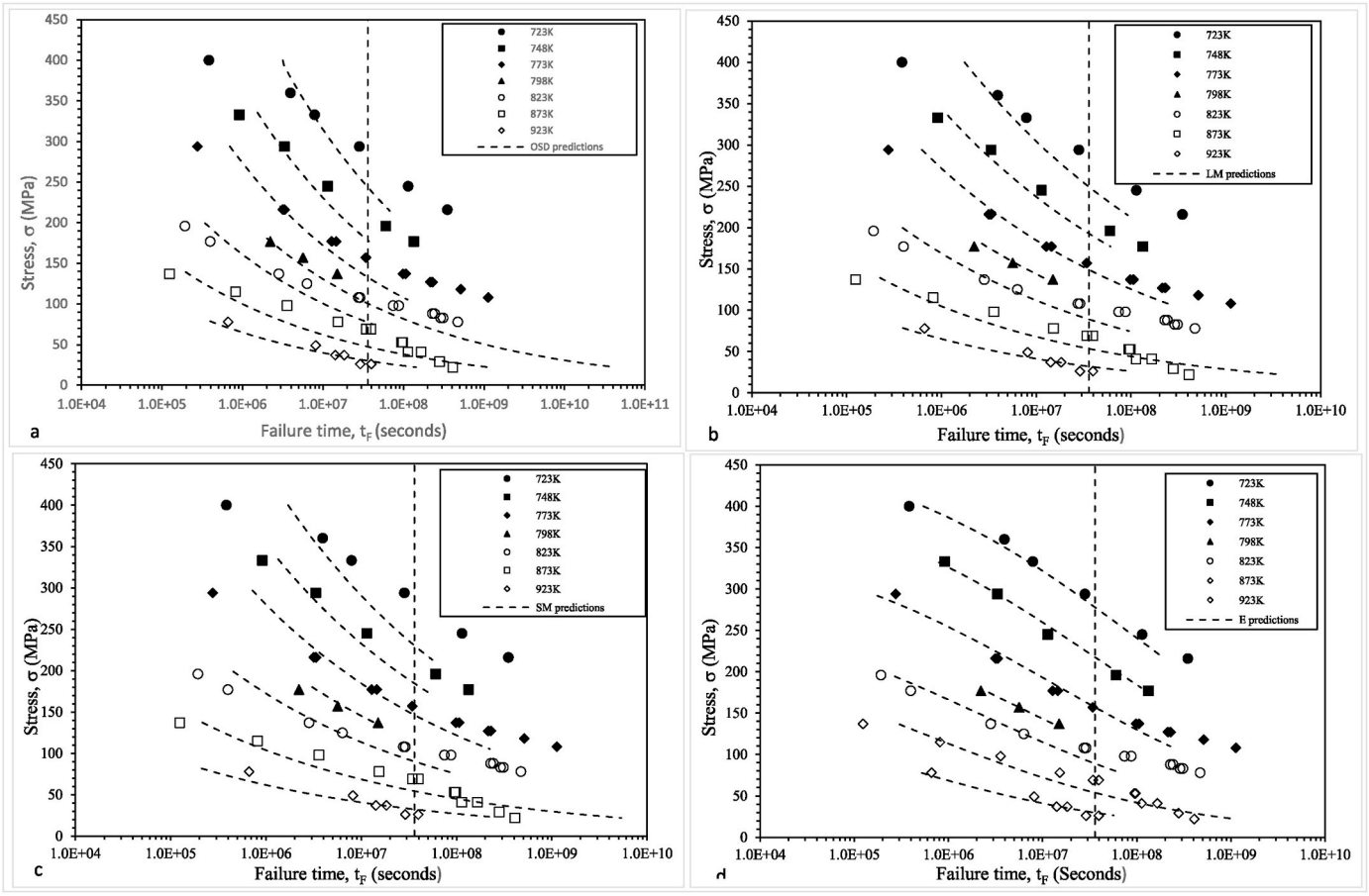

Fig. 6. Predictions of t_F at various stresses and temperatures together with the actual failure times (predictions based on data with $t_F < 10{,}000$ h) using (a) the OSD model, (b) the LM model, (c) the Soviet model and (d) the Evans model.

The results of using this LOESS technique to model the temperature compensated failure times for the same four models as in section 3.3 are shown in Fig. 7. Compared to the parametric predictions shown in Fig. 4, the data are more tightly compacted around now non-linear, smooth, and quite complex shaped prediction curves - as reflected in a much smaller Z_p values. The 90% confidence bands for the temperature compensated failure times are therefore much smaller. For the OSD model, CV was minimised at 0.0743 using the 8 nearest data points to each x_0 and using only those stresses inducing a failure time of 10,000 h or less. The activation energy used for temperature compensating the failure times was estimated at 349 kJmol^{-1}, which is very close to the activation energy for lattice self-diffusion in α-iron of around 350 kJ mol^{-1} [20]. As such, LOESS seems to produce a more sensible Q_c value (compared to the parametric approach of section 3.3 where $Q_c = 279$ kJmol^{-1}). Norton's slope parameter n at each stress value is shown in Fig. 8a, the intercept parameter $\ln(B) + \frac{Q_c}{R}\left(\frac{1}{T_0}\right)$ at each stress value is shown in Fig. 9a.

For the LM model, CV was minimised at 0.0701 using the 8 nearest data points to each x_0 using only those stresses inducing a failure time of 10,000 h or less. The parameter (ln(A*)) used for temperature compensating the failure times was estimated at −34.977 – which is similar in value to that obtained using the parametric approach. The slope parameter a_1/RT_o obtained at each stress value is shown in Fig. 8b, the intercept parameter $\ln(A^*) + \frac{a_0}{R}\frac{1}{T_o}$ at each stress value is shown in Fig. 9b.

For the SM model, CV was minimised at 0.0999 using the 7 nearest data points to each x_0 using only those stresses inducing a failure time of 10,000 h or less. The parameters ($a_4 + a_5$ and Q_c) used for temperature compensating the failure times were estimated at 25.34 and 607kJmol^{-1} respectively – which are quite different in value to those obtained using the parametric approach. The slope parameter $a_5 + \frac{a_6}{T_o}$ obtained at each stress value is shown in Fig. 8c, the intercept parameter $\ln(D) + a_4 \ln(T_o) + Q_c\frac{1}{RT_o}$ at each stress value is shown in Fig. 9c

For the Evans model, CV was minimised at 0.0121 using the 10 nearest data points to each x_0 using only those stresses inducing a failure time of 10,000 h or less. The activation energy used for temperature compensating the failure times was estimated at 268 kJmol^{-1} which is similar in value to that used by Wilshire and Whittaker [4]. The slope parameter n* obtained at each stress value is shown in Fig. 8d, the intercept parameter $\ln(B^*) + \frac{Q_c}{R}\frac{1}{T_o}$ at each stress value is shown in Fig. 9d. The estimated values for σ_{max} shown in Fig. 7d are also interesting. At 923 K, σ_{max} is much larger than the reported tensile strengths. Evans [12] explained this pattern in terms of the strain rate dependency of the tensile strength at high temperatures. Namely that at temperature of 923 K or more, the strain rate used by NIMS was inappropriate for determining the deadload stress leading to instantaneous failure.

4.2. Deformation mechanisms and LOESS parameter variation in the Evans model

Fig. 8d & 9d tend to suggest different stress and control of dislocation motion regimes that are broadly consistent with the findings of Maruyama et al. [1] and Wilshire and Whittaker [4]. As discussed in the introduction section when at the lowest stresses, the resulting long nature of the tests results in the creep process degrading the initial bainitic microstructures, such that the original lath-like structure entirely

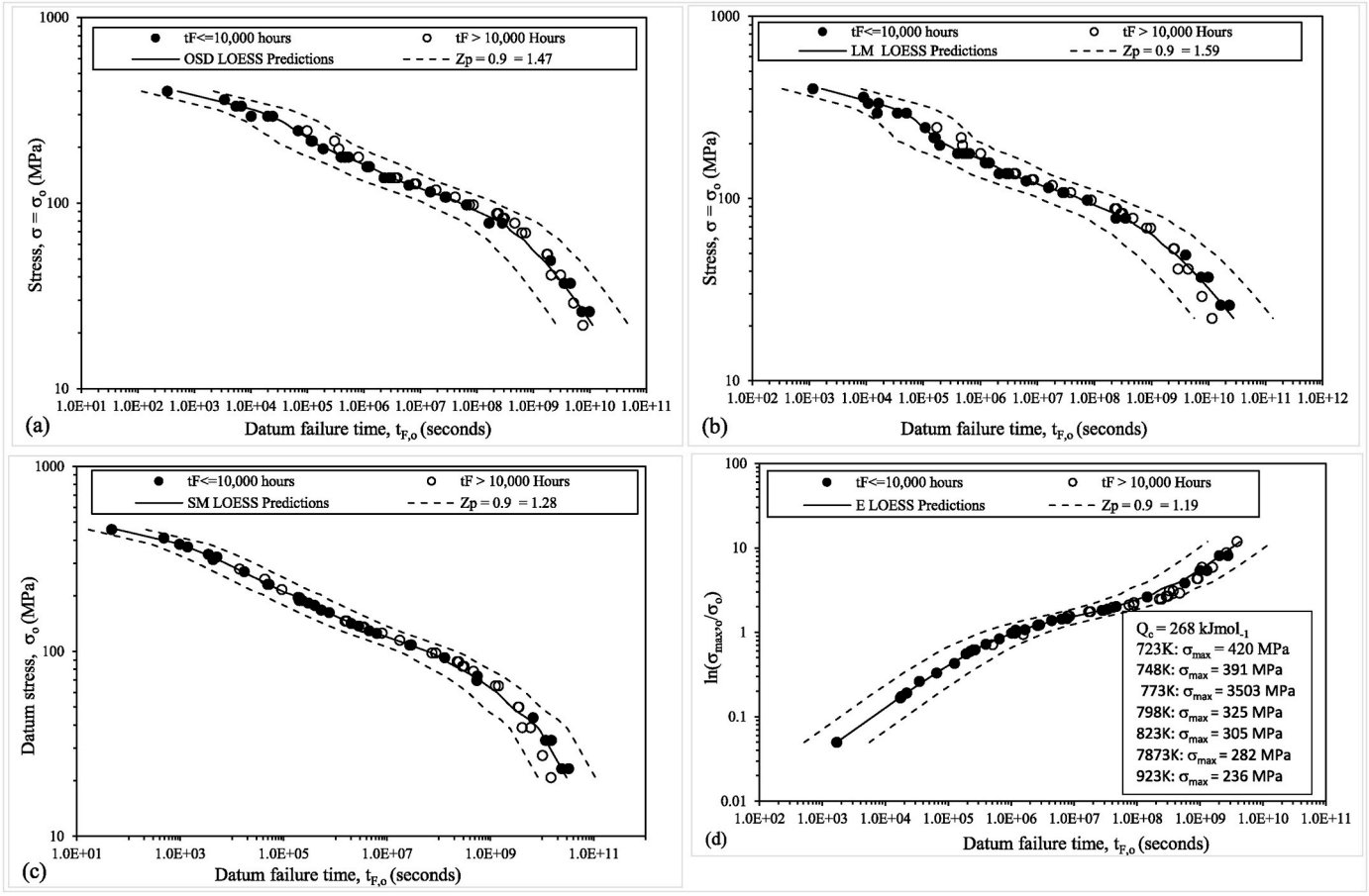

Fig. 7. LOESS predictions for temperature compensated failure times $t_{F,0}$ obtained using (a) the OSD model, (b) the LM model, (c) the Soviet model and (d) the Evans model.

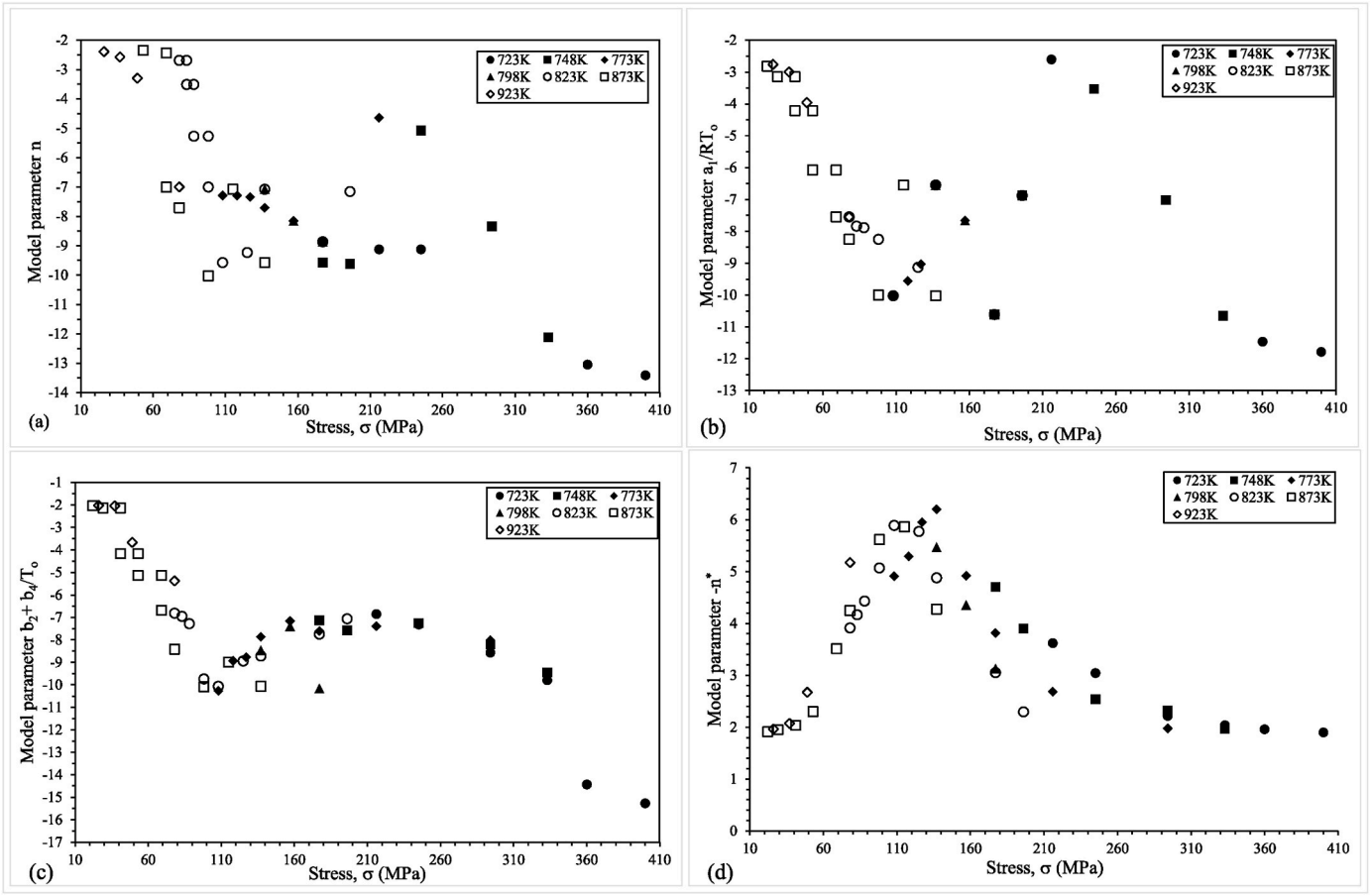

Fig. 8. Variation in the "slope" parameter with stress for (a) the OSD model, (b) the LM model, (c) the Soviet model and (d) the Evans model.

disappears. This gives fast creep rates. This reflects itself in the low values for n* in Fig. 8d (n* of around 2) at stresses of 60 MPa or less, i.e., any reduction in stress will only results in small increases in life due to the creep rates being very high in this stress regime. Then at more intermediate stresses of between 60 and 110 MPa (but still below the yield stress), creep occurs mainly by the movement of the dislocations pre-existing in the as received bainitic microstructure and the non-degraded microstructure allows precipitates to effectively slow down the rate of creep compared to the low stress regime. This reflects itself in the higher values for n* in Fig. 8d - n* transitions to a value of around 6 as the stress increase from 60 MPa towards 110 MPa). Any reduction in stress will now result in larger increases in life (hence the higher value for n*) due to the creep rates being slower in this stress regime compared to the low stress regime. Finally, at the very highest stresses above 110 MPa dislocations multiply rapidly during the initial strain upon high loading, giving higher creep rates than in the intermediate stress regime. This reflects itself in falling values for n* in Fig. 8d (n* tends to return to around 2 with increasing stress) at stresses above 110 MPa, i.e., any reduction in stress will now only results in small increases in life due to the creep rates being once again very high in this high stress regime.

Fig. 9d shows of the intercept (i.e., the value for $\left\{\ln(B^*) + \frac{Q_c}{R}\frac{1}{T_o}\right\}$) of the Evans model at different test conditions. Like n* it has three distinct regimes, taking on a value of around 17.5 at the lowest stress and a value of around 14 above 110 MPa. The intermediate stress range sees the transition in this intercept value.

Whilst these changing parameter values are not able to reveal the role of primary creep on time to failure, the changes in parameter values in Fig. 8d & 9d attributed above to microstructure evolution do, according to Wilshire and Whittaker [4], suggest the need to focus on tertiary creep and damage accumulation. These authors suggest that the presence of a minimum rather than a secondary creep rate suggests that to explain failure times, attention should be focussed on the deformation processes governing strain accumulation and the damage phenomena causing the tertiary acceleration and eventual fracture. They argue that dominant dislocation processes controlling creep are the same as the bainitic microstructures degrades but the phenomena causing the onset of tertiary creep and eventual fracture differ with test conditions. Their analysis of this NIMS data lead them to conclude that tertiary creep begins by necking at 773 K and by microstructural instability at the higher temperatures, leading to *trans*-granular fracture. When $\sigma < 150$ MPa a transition in failure mode to creep cavitation begins but even then, cavity development is limited by grain boundary migration in the degraded microstructure at low stresses at 873 K and above.

4.3. Semi-parametric (LOESS) extrapolated failure times

Fig. 10 illustrates how the LOESS technique, when used within the Evans model, extrapolates to predict the failure time measured at 873 K and 22 MPa using only data points with failure times of 10,0000 h or less. For this model the activation energy was estimated at 268 kJmol^{-1} (see in Fig. 7d) and so using the terminology of the appendix section, $y_i = \ln(t_{F,o}) = \ln(t_F) - (268{,}000/8.314)[(1/T - 1/823)]$. The actual value for y at 873 K and 22 MPa is therefore $y_o = 19.8278 - (268{,}000/8.314)[(1/873–1/823)] = 22.073$. For this model, σ_{max} at 873 K is estimated at 282 MPa (see in Fig. 7d) and so and $x_i = \ln\left(\frac{282}{\sigma} - 1\right)$. At 873 K and 22 MPa, $x_0 = \ln\left(\frac{282}{\sigma} - 1\right) = 2.4709$. The solid triangle in Fig. 10 shows this y_o, x_o pairing. The solid circles are the 10 values (as CV was found to be minimised for this bandwidth value) for x that are closest to x_o, i.e., that have the 10 smallest $|x_i - 2.4709|$ values and have t_F less than 10,000 h.

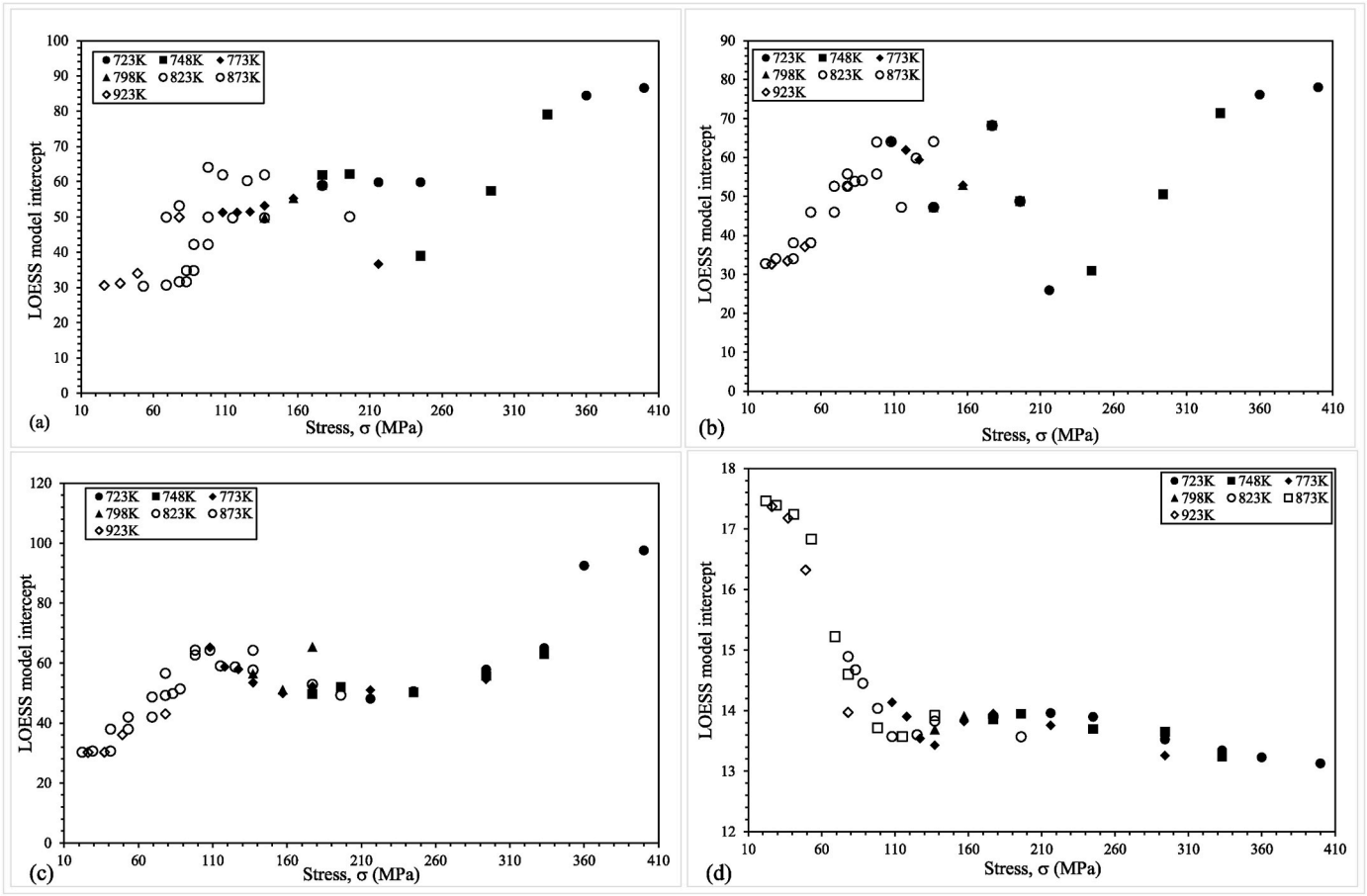

Fig. 9. Variation in the "intercept" parameter with stress for (a) the OSD model, (b) the LM model, (c) the Soviet model and (d) the Evans model.

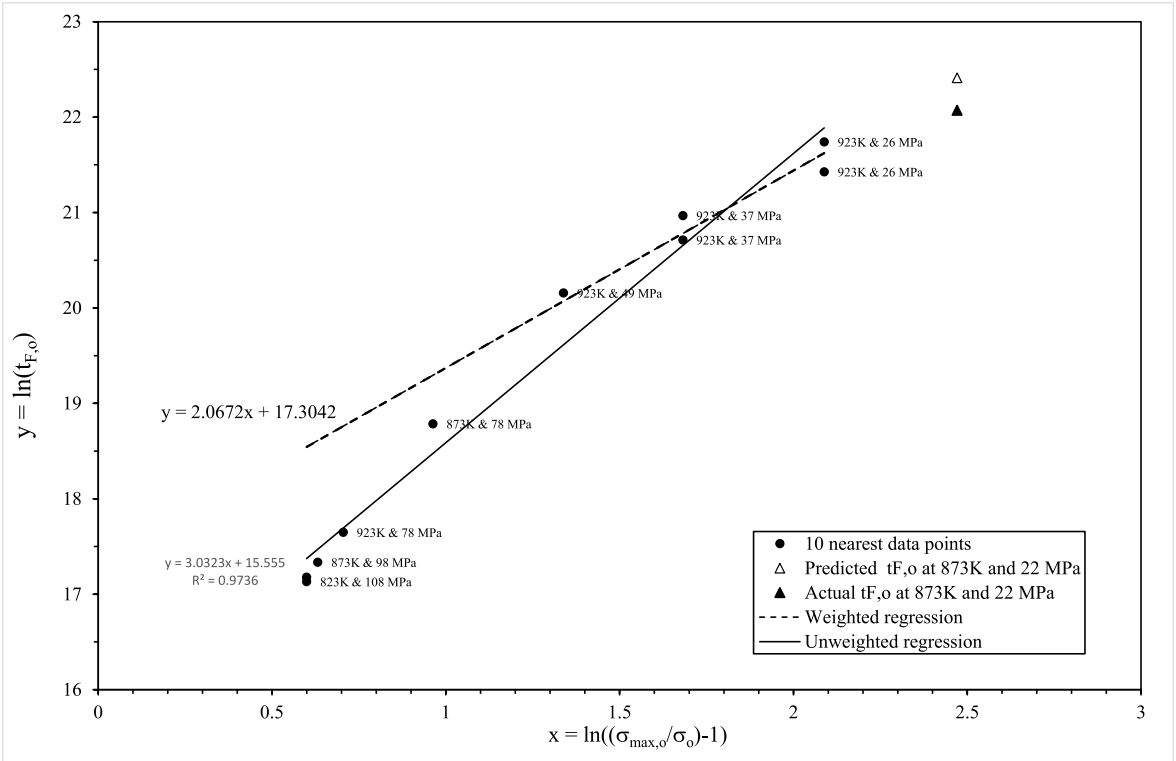

Fig. 10. Illustrating the LOESS technique in the Evans model for predicting the time to failure at 22 MPa and 873 K.

Thus, only the short-term data is used in predicting the failure time at 873 K and 22 MPa. The solid line is then the best fit line through these 10 data points and the dashed line is the weighted best fit line – where the weights are given by the square root of Eq. (A2). As the weights associated with the two tests caried out at 823 K and 108 MPa were zero by this equation, the weighted line used just the nearest 8 data points. The predicted value for $t_{F,o}$, shown as the open triangle in Fig. 10, is obtained by extrapolating this weighted best fit line: 2.0672(2.4709)+17.3042 = 22.4122.

It is clear from this illustration that extrapolation to any stress below 22 MPa is possible, and that extrapolation with respect to temperature is just based on the Arrhenius equation, i.e., $\ln(t_F) = 22.4122+(268{,}000/8.314)[(1/873–1/823)] = 20.1699$. Further, the failure time at 22 MPa for any other temperature is found by simply replacing 873 in the last calculation shown with the required temperature. Repeating these calculations for the solid circles shown in Fig. 7d yields the smooth prediction curve shown in this figure. Repeating it for the data points shown as open circles in Fig. 7d, i.e., where failure time exceeds 10,000 h) yields the predictions shown in Fig. 11d which are plotted against the actual failure times.

Applying this procedure to all the failure times more than 10,000 h yields the results shown in Fig. 11. All four models have very similar $Z_{p=0.9}$ values ranging from 1.58 for the OSD model to 1.98 for the LM model. But all have 90% confidence limits slightly outside the ideal requirement of 1.55. The nature of these extrapolations is slightly different in each case however, as revealed by the fitted trend lines shown in Fig. 11. In the OSD model this trend line is always above the 45° line and so this model has a tendency on average to always under predict the time to failure. In the other 3 models however the trend lines approaches or crosses below the 45° lines with increasing failure times. As such there is a tendency to under predict on the average at the smaller failure times, but this bias diminishes (or reverses) as the failure time increases. That is, these models will give better predictions at stresses closer to the operating stress at a given temperature. But for all models, the LOESS failure time predictions are much better than the parametric predictions as revealed through a comparison of Fig. 11 with Fig. 5. The trend lines are now much closer to the ideal 45° lines.

Fig. 12 reveals these differences in the more familiar stress v time space. The SM and E models predict best at the lowest two temperatures. All four models appear to produce similar and very good predictions at 773 K. At 823 K, all models tend to under predict, but this is worse in the SM and E models. At 873 K the E model produces the most accurate predictions, whilst the othe models tend to over predict. Also, the isothermal predictions are now smooth curves more reflective of gradually evolving creep mechanisms and are not like the awkward looking isothermal predictions typically associated with, for example, the Wilshire model – where there are abrupt and discontinuous break points and various stresses. Using the Evans model, and in comparison, to Fig. 6, the large under predictions at the lowest stresses at each temperature are now largely removed – except at the very lowest stresses at 823 K.

5. Conclusions

This paper has demonstrated the inadequacy of some commonly used parametric creep models when it comes to both representing 2.25Cr–1Mo failure times and when it comes to predicting failure times close to operating conditions when using only accelerated test data. For

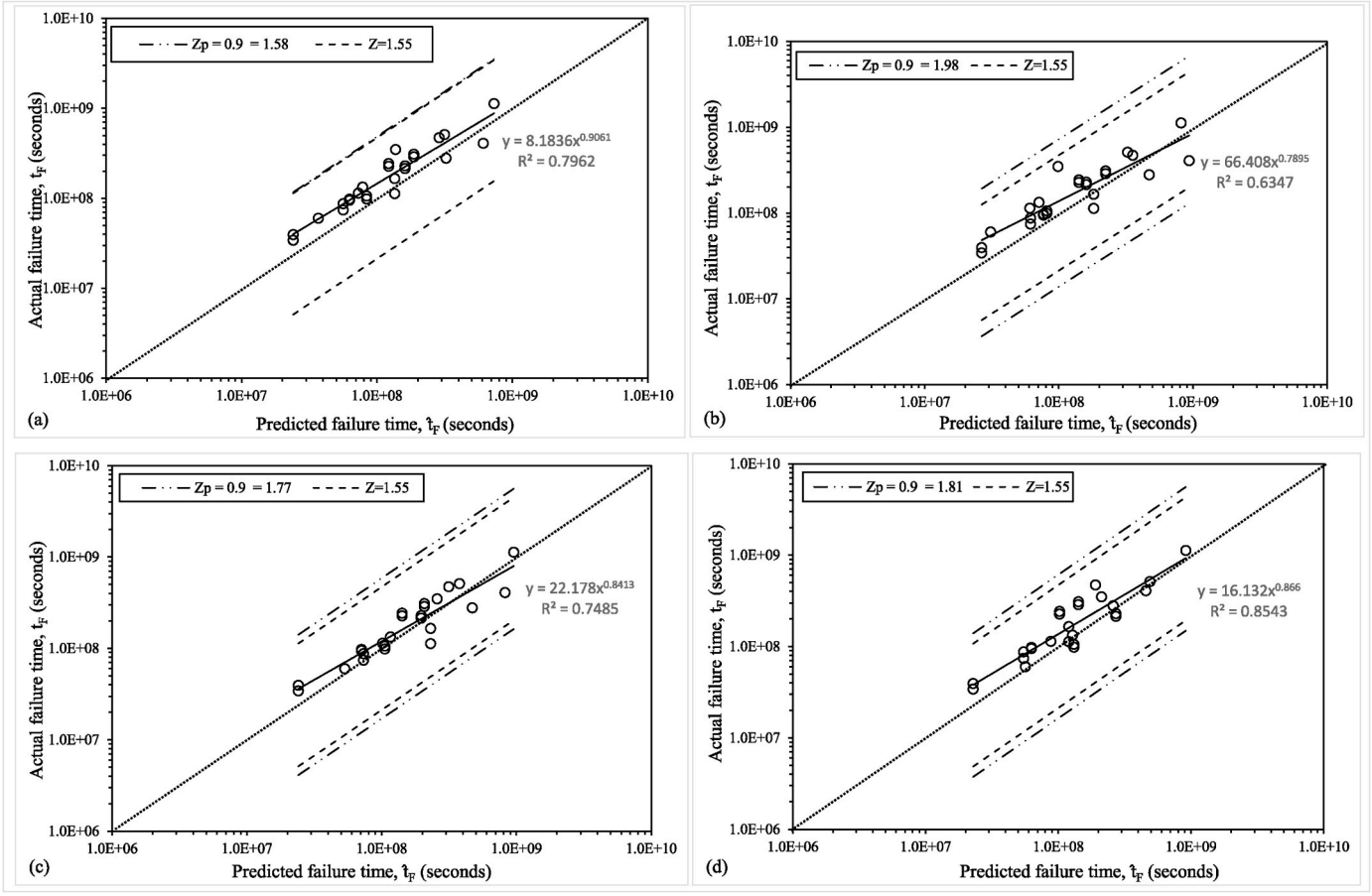

Fig. 11. Showing the actual v LOESS predicted t_F values beyond 10,000 h for (a) the OSD model, (b) the LM model, (c) the Soviet model and (d) the Evans model (these models are estimated using t_F values less than 10,000 h).

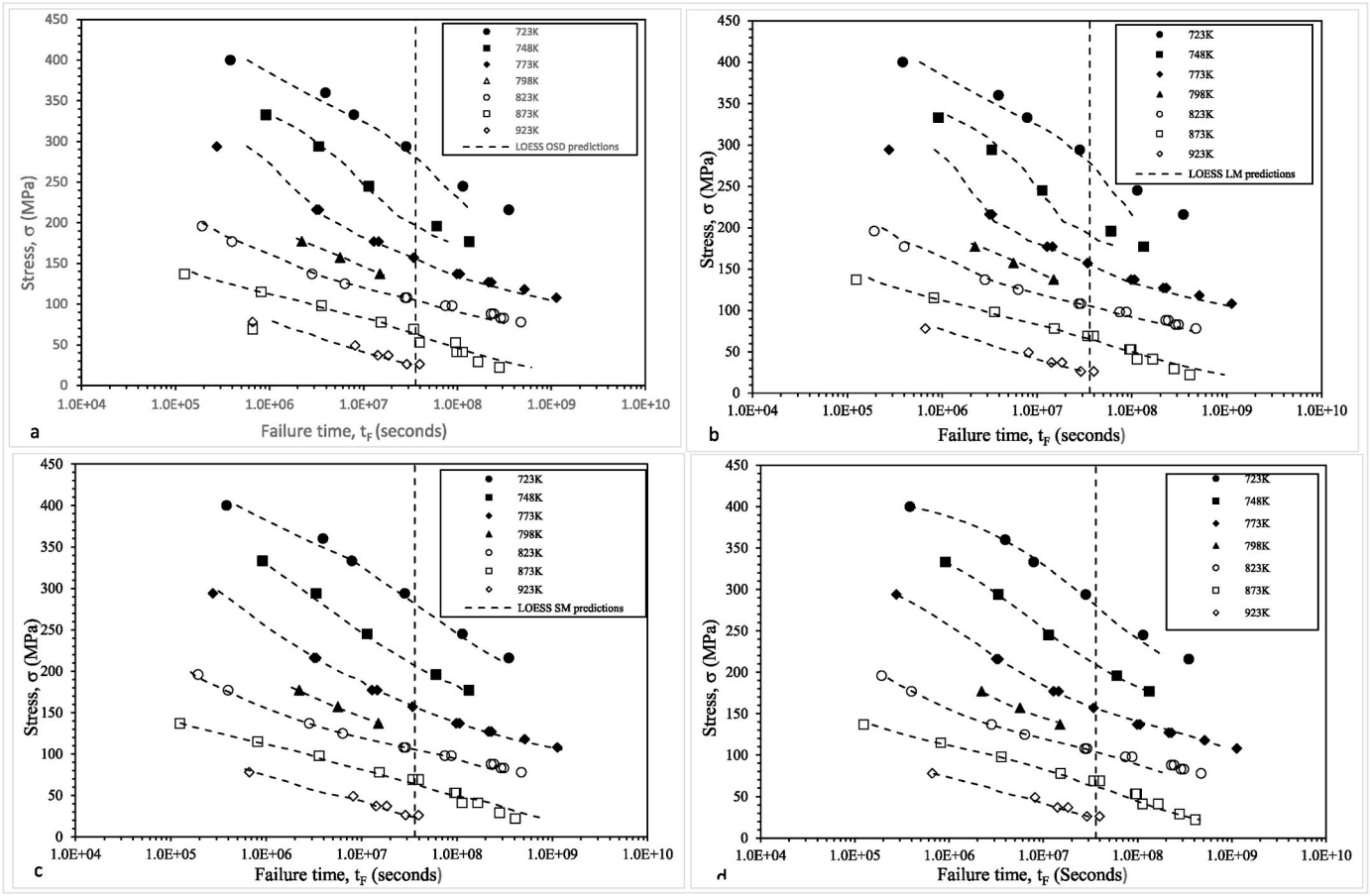

Fig. 12. LOESS predictions of t_F at various stresses and temperatures together with the actual failure times (predictions based on data with $t_F < 10{,}000$ h) using (a) the OSD model, (b) the LM model, (c) the Soviet model and (d) the Evans model.

2.25Cr–1Mo steel this is explained by changing creep mechanisms with respect to stress, so that such parametric models are only plausible over a narrow or local range of test conditions where the creep mechanism is constant. The paper then introduces a semi-parametric estimation procedure (LOESS) that can be used to deal with changing creep mechanisms whilst maintaining the structure of the parametric model.

When applied to 2.25Cr–1Mo steel it was found that the model parameters varied in line with changing creep mechanisms already identified in the literature for this material, and that the estimated activation energy was closer to that for self-diffusion in this material. Also, all the models estimated via this LOESS procedure seemed to better represent the experimental failure times compared to parametric estimation, and the longer-term predictions from short term data were also much improved. Areas for future work include applying this technique to other steels and high temperature materials and extending the approach to allow the parameters that temperature compensate failure times and stresses to also vary with test conditions. For example, it is known that for many metals operating at high temperatures there are at least two activation processes, (lattice diffusion and boundary diffusion). And so, it would be of interest to modify the LOESS technique discussed in this paper to allow for different activation energies at different test conditions and to determine if such a generalisation results in superior lifetime predictions.

Data

All data used in this publication are in the public domain: References [2,3].

Declaration of competing interest

The authors declare that they have no known competing financial interests or personal relationships that could have appeared to influence the work reported in this paper.This research was not funded by research council grants or private sponsors and as such there are no financial relationships to declare.

Data availability

The data is in the public domain

Appendix

One way to preserve the structure of a parametric creep model whilst improving their predictive power is to accept that these models are realistic descriptors of creep over only a narrow range of test conditions, i.e., over conditions where the creep mechanism remains unchanged, and then apply a locally weighted estimation technique (LOESS) over this reduced range. Local is defined as only those test conditions closest to a test condition of interest – the so-called target test. To illustrate further, let variable $y = \ln(t_{F,o})$ and variable $x = \ln(\sigma_o)$. As such the values for y and x are determined by the creep model selected and their quantification will require estimating unknown parameters. Then, and closely following the method outlined by

Cleveland [7], a Kernel is used to identify the weights $w(x_i, x_o)$ to be used in the local regression

$$w(x_i, x_o) = K_h(x_i, x_0) = K_h\left(\frac{|x_i - x_o|}{h}\right) \tag{A1}$$

where h is the bandwidth, x_i is the ith value for x (of which there are Q) and x_o is a target value for x – one of the Q values for x. Clearly, K_h and w are implicitly dependent on both x_i and x_o and so each x_o has its own Kernel values (so for example, $K_h(x_i, x_0)$ reads the value for K_h when $x = x_i$ and when using x_o as the target value for x).

The bandwidth can be specified in many ways, but for LOESS, the value for h changes as a function of x_o, so that the number of points inside ($x_o - h$, $x_o + h$) remains constant. One advantage of this approach is that h is then interpretable as the fraction (q) of the sample of data (Q) used in constructing the local fit around any point x_o. This fraction remains the same for all selected x_o values. In this approach, a value for x is selected and assigned to the variable x_o. The absolute distances $|x_i - x_o|$ are then calculated. If only half of the x_i values are going to be used in the local regression, then h becomes equal to the median value for $|x_i - x_o|$. If only a quarter of the x_i values are used, then h becomes equal to the lower quartile value for $|x_i - x_o|$. In general h is equal to a percentile of $|x_i - x_o|$, where the percentile is equal to the proportion of the sample of data used in the local regression. This is repeated by changing x_o to another value of x_i, until all values for x_i have been made x_o. This will lead to the creation of Q K_h functions, each containing Qq separate values.

K_h must be a continuous function and there are many commonly used Kernels in the literature, but the one proposed by Cleveland, is the tri-cubic Kernel

$$w(x_i, x_o) = K_h(x_i, x_0) = \begin{cases} \left(1 - \left(\frac{|x_i - x_o|}{h}\right)^3\right)^3 & \text{when } \left|\frac{x_i - x_o}{h}\right| < 1 \\ 0 \quad \text{otherwsie} \end{cases} \tag{A2}$$

So, for a selected target value x_o, the following weighted regression is carried out using the least squares method

$$y_i \sqrt{w(x_i, x_o)} = a(x_o) \sqrt{w(x_i, x_o)} + b(xo)\sqrt{w(x_i, x_o)} \tag{A3}$$

to obtain values for a and b associated with the target value x_o ($b(x_o)$ reads the estimated value for b using x_o as the target). The predicted value for y associated with each x_o is then given by

$$\hat{y}(x_o) = a(x_o) + b(x_o)xo \tag{A4a}$$

Notice this can also be used to predict a value for y at other values for x around x_o by replacing x_o with x_i

$$\hat{y}(x_i) = a(x_o) + b(x_o)x_i \text{ for all } x_i \text{ within the band width} \tag{A4b}$$

These calculations are repeated for every value for x_i (by each time making x_o equal to each x_i). So, not only is the sample size reduced, but weighting of the data points also takes place within this reduced more local sample. This modification of the Kernel, termed automatic Kernel carpentry, eliminates the bias present in the Nadaraya-Watson Kernel [21]. In combination, this should ensure only data points that have the same data generating mechanism (i.e., creep mechanism) are used to estimate the parameters a and b. Plotting the variation in a and b associated with each x_o will then reveal any change in creep mechanism – i.e., that leads to a change in the values for a and b.

The only remaining unknown is the bandwidth itself, i.e. what should be the value for h? Generally, this is chosen using "leave one data point out cross validation". In this approach Equation (A3) is replaced with

$$y_i \sqrt{w(x_i, x_o)} = a(x_o) \sqrt{w(x_i, x_o)} + b(x_o)x_i \sqrt{w(x_i, x_o)} + d(x_o)D_i \tag{A5}$$

where D_i is a dummy variable that equals 1 when $x_i = x_o$ and zero otherwise. The parameter d can then be interpreted as the error made in predicting that value for y obtained at test condition x_o when this y and x_o data pairing are not used in the estimation of a and b in equation (A3). Such a value for d can be computed for all $x_o = x_i$, squared and then summed to obtain the sum of squared cross validation errors (CV)

$$CV = \sum_{i=1}^{Q} d(x_o)_i^2 \tag{A6}$$

The bandwidth h is then taken to be that value which minimise CV. An alternative to this is to use generalised cross validation (GSV). In this approach, for each x_o, the following loadings are calculated

$$L_i(x_o) = 1 - \sqrt{[y(x_o) - \hat{y}(x_o)]/d(x_o)_i^2} \tag{A7}$$

If v is the average of these loadings, then

$$GSV = \frac{1}{Q}\sum_{i=1}^{Q}\left[\frac{(y_i - \hat{y}_i)}{1 - v}\right]^2 \tag{A8}$$

and h can be chosen so at to minimise GSV. The advantage of this approach is that GSV is approximately proportional to the Akaike Information Criteria or AIC [22], which balances the degree of fit with the number of degrees of freedom. In this approximation, v acts as the effective degrees of freedom. Clearly, these two approaches will give more similar values for h the less spread there is in the values for $L_i(x_o)$. Excel's Solver [17] is used to search for the value for the parameters that temperature compensate failure times (ti fing values for yi) that minimises the sum sqaured residuals calculated from the Q applications of linear least squares to equation (A5).

References

[1] K. Maruyama, K. Sawada, J. Koike, H. Sato, K. Yagi, Examination of deformation mechanism maps in 2.25Cr—1Mo steel by creep tests at strain rates of 10−11 to 10−6 s−1, Mater. Sci. Eng. A224 (1997), 166- I72.

[2] NIMS Creep Data Sheet No. 3B: Data Sheets on the Elevated-Temperature Properties of 2.25Cr-1Mo Steel for Boiler and Heat Exchanger Seamless Tubes (STBA 24), National Research Institute for Metals, Tokyo, Japan.

[3] NIMS Creep Data Sheet No.50A: Long-Term Creep Rupture Data Obtained after Publishing the Final Edition of the Creep Data Sheets, National Research Institute for Metals, Tokyo, Japan.

[4] B. Wilshire, M. Whittaker, Long term creep life prediction for Grade 22 (2·25Cr-1Mo) steels, Mater. Sci. Technol. 27 (3) (2011) 642–647.

[5] Y.P. Ding, X.J. Wu, R. Liu, X.Z. Zhang, F. Khelfaoui, Creep performance characterization for Haynes 282TM using the deformation-mechanism-based true stress model, Therm. Sci. Eng. Prog. 36 (2023), 101603.

[6] J. Bolton, Rupture modelling and extrapolation of a sparse dataset for Inconel 740H, Int. J. Pres. Ves. Pip. 194 (B) (2021), 104543.

[7] W.S. Cleveland, Robust locally weighted regression and smoothing scatterplots, J. Am. Stat. Assoc. 74 (1979) 829–836.

[8] J.E. Dorn, L.A. Shepherd, What we need to know about creep, in: Proceedings of the STP 165 Symposium on the Effect of Cyclical Heating and Stressing on Metals at Elevated Temperatures, 1954. Chicago, IL, USA, 17 June.

[9] F.R. Larson, J.A. Miller, Time temperature relationship for rupture and creep stresses, Trans. ASME 174 (1952) 5.

[10] F.C. Monkman, N.J. Grant, An empirical relationship between rupture life and minimum creep rate in creep-rupture tests, Proc. Am. Soc. Test. Mater. 56 (1956) 593–620.

[11] S.S. Manson, A.M. Haferd, A linear time-temperature relation for extrapolation of creep and stress-rupture data, NACA Technical Note 2890; National Advisory Committee for Aeronautics: Cleveland, OH, USA, 1953. Materials 10 (2017), 1190 29 of 30 15.

[12] Evans, M. The Critical Role Played by High Temperature Tensile Testing in the Accurate Assessment of Creep Life Using Wilshire Type Creep Models, Metallurgical and Materials Transactions A, (Forthcoming)..

[13] H. Eyring, The activated complex in chemical reactions, J. Chem. Phys. 3 (2) (1935) 107–115.

[14] S.S. Manson, U. Muraldihan, Analysis of creep rupture data in five multi heat alloys by minimum commitment method using double heat term centring techniques, in: Progress in Analysis of Fatigue and Stress Rupture MPC-23, ASME, New York, NY, USA, 1983, pp. 1–46.

[15] J.A. Cano, M.S. Haque, M.A. Hossain, C.M. Stewart, Accelerated qualification of creep-resistant materials using a datum temperature method (DTM) to calibration, Int. J. Pres. Ves. Pip. 199 (2022), 104746.

[16] I.I. Trunin, N.G. Golobova, E.A. Loginov, New methods of extrapolation of creep test and long time strength results, in: Proceedings of the 4th International Symposium on Heat Resistant Metallic Materials, Mala Fatra, Czechoslovakia, 1971.

[17] Microsoft Corporation, Microsoft Excel [Internet], Available from: https://office.microsoft.com/excel, 2018.

[18] S.R. Holdsworth, B. Askins, M.A. Baker, E. Gariboldi, S. Holmström, A. Klenkf, M. Mingelf, Z. Merckling, R. Sandstromh, G. R, N. Schwienheeri, S. Spigarellij, Factors influencing creep model equation selection, Int. J. Pres. Ves. Pip. 85 (1–2) (2008) 80–88.

[19] S.R. Holdsworth, Developments in the assessment of creep strain and ductility data, Mater. A. T. High. Temp. 21 (1) (2004) 125–132.

[20] B. Miilion, J. Kucera, Korore Mater 22 (1984) 372.

[21] E.A. Nadaraya, Nonparametric estimates of density functions and regression curves, Theor. Probab. Appl. 10 (1965) 186–190.